Coupling between dynamic slowing down and chemical heterogeneity in a metallic undercooled liquid

N. Jakse and A. Pasturel
Univ. Grenoble Alpes, CNRS, Grenoble INP, SIMaP, F-38000 Grenoble, France
(Received 5 February 2017; revised manuscript received 21 March 2017; published 28 April 2017)

We investigate the connection between local structure and dynamics in the liquid and undercooled $Al_{93}Cr_7$ alloy using *ab initio* molecular dynamics simulations. In the liquid phase, we show the striking effects of Cr alloying on the atomic-scale structure, characterized by a heterogeneous local ordering around each component, due to a strong interplay between chemical short-range order and icosahedral short-range order. In the undercooled phase, this interplay leads to the formation of an icosahedral-based medium-range order (IMRO) referring to Cr atoms. In examining the dynamic properties, we observe that this chemically induced structural heterogeneity gives rise to a substantial decoupling of component diffusion in the liquid phase, far above the liquidus temperature. In the undercooled regime, we find the breakdown of the Stokes-Einstein relation and a pronounced increase of the non-Gaussian parameter, indicating the onset of dynamic heterogeneities. Using the isoconfigurational ensemble method, we evidence that the structural origin of dynamics heterogeneities is clearly related to the formation of IMRO. Finally, we discuss the role played by IMRO in nucleation on the preexisting icosahedral cluster in the liquid phase.

DOI: 10.1103/PhysRevB.95.144210

I. INTRODUCTION

Understanding dynamics in liquids upon undercooling represents one of the major challenges in condensed matter. Perhaps the most striking feature is the increase in viscosity and relaxation time of liquids towards the glass-transition temperature, T_g, despite little change in their static structure, in contrast with crystallization.

The increasing rate of viscosity with falling temperature down in the deep undercooling regime has been used by Angell [1] to classify liquids by introducing the concept of fragility. A liquid is called strong or fragile depending on the change in viscosity as a function of temperature. Viscosity of strong liquids exhibits an Arrhenius-temperature dependence, $\eta = \eta_0 \exp(E/k_B T)$ where η_0 is a constant and E is an effective activation energy. For fragile liquids, E is not constant when the temperature decreases and a good fit of viscosity is given by the Vogel-Fulcher-Tammann (VFT) law, $\eta = \eta_0 \exp[BT_0/(T - T_0)]$ where η_0 and B are material-dependent parameters. Note that the divergence of viscosity at a finite temperature, T_0, is not a prerequisite to obtain a good representation of experimental data [2].

Another interesting feature of undercooled liquids is that their dynamics results from microscopic cooperative processes. Both experimental and numerical studies [3–8] have revealed that a liquid does not fall into a glass in a spatially homogeneous fashion because near the glass-transition temperature, the rates of atomic rearrangements can differ by orders of magnitude from one region of space to another [4,6]. This phenomenon, called "spatially heterogeneous dynamics" or dynamic heterogeneities (DHs), may evolve over time since undercooled liquids are ergodic systems; a slow region will eventually become fast and vice versa. DHs are apparently a universal feature of undercooled liquids since they have been observed for strong as well as fragile liquids [9,10].

Furthermore, the presence of DHs has been argued to give rise to the decoupling of the self-diffusion (D_S) and viscosity and then to the breakdown of the Stokes-Einstein (SE) relation, $D_S\eta/T = cste$ [10]. Specifically, the breakdown of the SE relation has been related to the particles in fast regions while particles in slow regions obey the SE relation [11]. However, some other studies indicate that the situation is much more complicated. For polymeric liquids, the dispersion of relaxation times is temperature independent and eliminates the possibility that DHs are at the origin of this decoupling [6]. Other contributions have shown that it is not necessary to use DHs to explain the breakdown of the SE relation [12–14]. Moreover, particles in both fast and slow regions were found to deviate from the SE relation [12,15].

The issue of the structural origin of DHs remains open for many systems and it is still debated as to whether there exists a static length scale that underlies the growing length scale for the dynamic correlations. To go beyond the pair correlations (or static structure factors) which usually display no significant changes as temperature decreases, many attempts have been proposed to identify locally favored structures and to investigate the change in population as a function of temperature [16–20]. For metallic liquids, structural motifs based on the fivefold symmetry or polyhedral ordering, as first suggested by Frank [21], have been used to present the glass transition as a frustration against crystallization. Within these approaches, frustration can be due to geometrical arguments [22], and random disorder effects or competing orderings [23]. However, the exact relationship of such polyhedral ordering to dynamic heterogeneities is still unclear even if measurements have shown that the polyhedral domains are slow to relax [24]. We note that even polyhedral ordering can be regarded as a structural motif in (quasi-) crystalline ground states like icosahedra in quasicrystal approximants [25]. Moreover, it has been suggested that critical-like fluctuations of the crystalline order are the origin of DHs in certain classes of undercooled liquids [26,27]. Let us mention that other recent attempts to identify structural features underlying the DHs have been proposed via various models such as the self-hole process [28], or through the concept of weakly effective particle [29]. Detection of icosahedral clusters up to the nanometer scale in a

metallic glass under stress and corresponding to the extension of the DHs has also been reported [30].

To unveil connections between structure and dynamics, it is tempting to link structural heterogeneity to dynamical heterogeneity. A causal link has been established on the basis of numerical simulations with the introduction of the isoconfigurational displacement (or propensity) field. A reasonable assumption is that stable structures should move less than unstable ones and in this manner, Widmer-Cooper and co-workers [31–33] showed that different local environments in the liquid structure lead to faster or slower relaxing regions, thus proving a structural origin for DHs. Note that within this approach, connections between liquid structure and liquid dynamics are all the more explicit that strong fluctuations in composition [34,35] or structure [25] are present.

In this paper, we address the important issue of the relation between structural and dynamic properties of the binary $Al_{93}Cr_7$ liquid upon undercooling by performing a series of first-principles molecular dynamics (AIMD) simulations as a function of temperature.

The main motivations to choose this system are that it belongs to one of the most representative class of materials, i.e., Al-based alloys, in which the crystallization of close-packed structures and the formation of quasicrystalline and amorphous structures compete as a function of the alloying composition and the cooling process [36,37]. Interestingly, Kurtuldu *et al.* [38,39] have recently shown that Cr addition in liquid Al-Zn alloys is believed to promote icosahedral short-range order (ISRO) in order to explain the refinement of the α-Al grain structure. Such an ISRO would lead to the formation of an Al-Cr icosahedral quasicrystal or a fragment of the stable approximant phase, Al_7Cr, which acts like a template for the nucleation of the α-Al phase upon cooling. Importantly, nucleation on this kind of quasicrystalline template may explain the remarkably high fraction of grain boundaries across which there is a twin or near-twin orientation relationship.

Finally we mention that this system has never been studied by molecular dynamics simulations and the presence of ISRO remains a merely speculative assumption in the absence of a direct experimental observation.

First, our findings show that the local structure is characterized by a strong Al-Cr affinity which favors the occurrence of the ISRO around Cr atoms, leading to different local ordering around each component. In the undercooled regime, this heteroatomic affinity causes the development of an icosahedral-based medium-range order (IMRO) referring to Cr atoms surrounded by Al atoms, which increases the structural heterogeneity at the atomic scale. In examining the dynamic properties, we observe that this chemically induced structural heterogeneity leads to a pronounced decoupling of component diffusion in the liquid phase, far above the liquidus temperature. In the undercooled regime, we find the breakdown of the Stokes-Einstein relation and a pronounced increase of the non-Gaussian parameter, indicating the onset of dynamic heterogeneities. Using the isoconfigurational ensemble method, we reveal that the structural origin of dynamics heterogeneities is clearly related to the formation of IMRO. In particular, we evidence that fast-dynamics regions are made up of only Al atoms while slow-dynamics regions are enriched in Cr atoms with respect to the chemical composition of $Al_{93}Cr_7$.

II. COMPUTATIONAL METHOD

AIMD simulations of liquid $Al_{93}Cr_7$ alloys were carried out using the Vienna *ab initio* simulation package (VASP) [40]. All the dynamical simulations were performed in the local density approximation [41] while the core-valence electron interaction was described by the projected augmented plane waves with a plane-wave cutoff of 270 eV. Newton's equations of motion were integrated using the Verlet algorithm in the velocity form with a time step of 1.5 fs within the *NVT* canonical ensemble by means of a Nosé thermostat to control temperature.

Some 256 atoms with the desirable composition are arranged in a cubic simulation box with standard periodic boundary conditions. Only the Γ point is used to sample the Brillouin zone. We have shown that such approximations reproduce the transport properties of liquid aluminum correctly [42].

The liquid samples were first prepared at a temperature well above the highest one studied to reach thermal equilibrium. This was followed by a cooling to the successive lower desired temperatures for the given alloy with a rate of 3×10^{12} K/s. We have considered height temperatures in the range going from 1400 to 700 K, the experimental liquidus temperature being close to 1000 K. At each temperature, the volume V of the simulation cell was chosen to reproduce the experimental densities [43]. The pressures calculated in the simulation cell do not exceed 0.9 GPa with a typical fluctuation of 1.2 GPa. Therefore, structural and dynamic properties are not influenced by pressure effects. Above the liquidus temperature, the run was continued for equilibration during a time up to 120 ps while 400 ps is used in the undercooled region. For $T = 700$ K, the equilibration was continued up to 700 ps. For each temperature, the equilibration time represents at least twice the relaxation time of the liquid alloy, which ensures the determination of structural and dynamic properties with a good statistical accuracy under equilibrium conditions [44]. For pure liquid Al, we have used our results from Ref. [43], which we have extended here in the temperature range between 1400 and 700 K. We also adopt the same procedure to describe structural and dynamic properties of pure liquid Cr in the temperature range between 2200 and 1700 K.

III. RESULTS AND DISCUSSION

A. Local ordering

At first, the structure of $Al_{93}Cr_7$ represented by the partial pair-correlation functions and a detailed three-dimensional image of the local ordering of each component provided by the common-neighbor analysis (CNA) [45] is routinely determined.

1. Partial pair-correlation functions

We computed the pair-correlation functions $g_{ij}(r)$ ($i, j =$ Al or Cr) from 1000 independent equilibrated configurations using standard techniques [46,47]. In Figs. 1(a)–1(c), we show the temperature dependence of $g_{ij}(r)$ up to the deep undercooling region.

Upon cooling, the first peak position remains essentially unchanged for Al-Al and Al-Cr partials ($r_{AlAl} = 2.74$ Å, $r_{AlCr} = 2.54$ Å) while it slightly increases for the Cr-Cr partial from

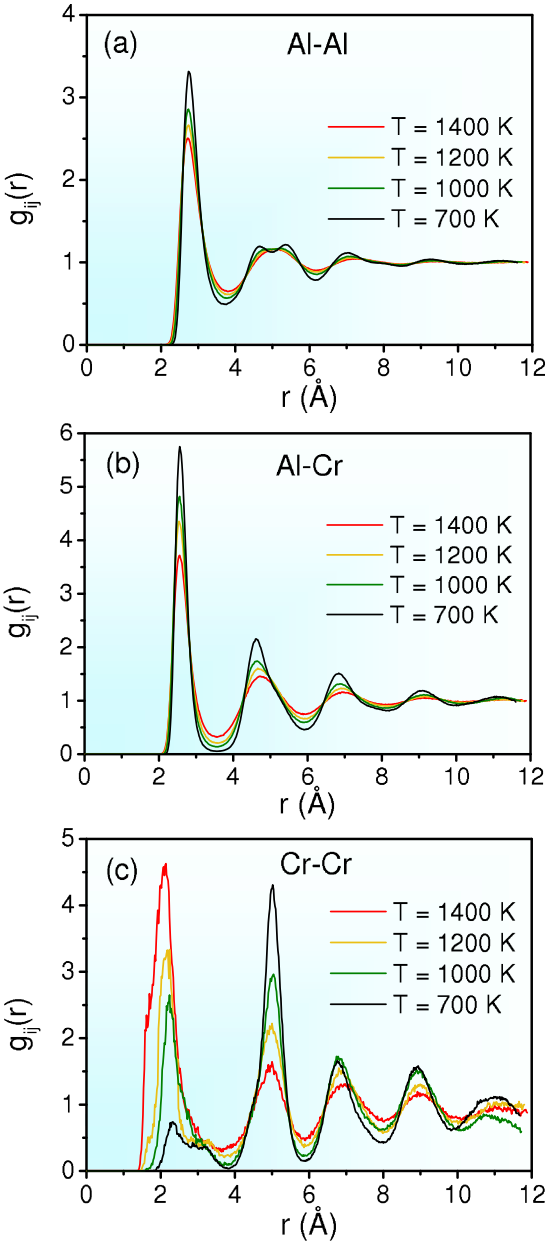

FIG. 1. Calculated partial pair-correlation functions from *ab initio* molecular dynamics simulations for temperatures $T = 1400$ K, 1200 K, 1000 K, and 700 K: (a) Al-Al, (b) Al-Cr, and (c) Cr-Cr.

$r_{CrCr} = 2.14$ Å at $T = 1400$ K to 2.24 Å at $T = 1000$ K. The most interesting feature concerns the intensities of the first and second peaks of the three partials and their evolution with temperature requires several comments. First, we note that the amplitude of $g_{AlCr}(r)$ becomes more and more pronounced with respect to $g_{AlAl}(r)$ and $g_{CrCr}(r)$ when temperature decreases below $T = 1300$ K, which is an indication of an increase of the heterocoordination in the alloy with preferred Al-Cr bonds, leading to the formation of a pronounced chemical short-range order (CSRO). Another indication of CSRO is the striking temperature dependence of the first peak of the Cr-Cr partial. Below 1000 K, it becomes lower than the second peak with a significant trend to disappear. As reported by Maret *et al.* from measured partial pair-correlation

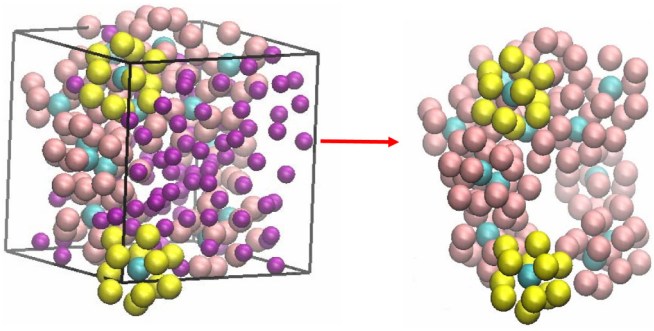

FIG. 2. Snapshot of the AIMD simulation showing a typical configuration at $T = 800$ K (left panel). Cr atoms are drawn in blue while Al atoms surrounding Cr atoms are light pink and the other Al atoms are shown in dark pink. Moreover, Al atoms in two typical Cr-centered icosahedra are highlighted in yellow as a guide for the eyes. For visual purposes, some of the atoms in the configuration are shown outside of the simulation cell by application of the periodic boundary conditions. The right panel shows the nearest-neighbor environment of Cr atoms extracted from the left-side configuration. It consists of a network of 160 atoms out of the 256 atoms with 142 Al atoms and 18 Cr atoms.

functions in liquid Al-based alloys [48] such a behavior is also in favor of an extension of chemical ordering to larger distances than the first Al-Cr one and can be related to the development of a medium-range order (MRO) referring to Cr atoms surrounded by Al atoms. Additionally, this MRO with the strong intermixing between Cr and Al atoms causes an increase of the structural heterogeneity at the atomic scale because Al atoms as the first-nearest neighbors of Cr atoms are less than Al atoms expected from the alloy composition.

To illustrate this structural heterogeneity, we show the atomic structure of a typical configuration obtained at 800 K in Fig. 2. The left panel evidences structural heterogeneities with regions made up by Cr atoms surrounded by their first-nearest neighbors and others with Al atoms only. The right panel shows the network formed by Cr atoms with their surrounding Al atoms, extracted from the simulation box shown on the left side.

Finally, note that the development of a shoulder in the second peak of $g_{AlAl}(r)$ and $g_{AlCr}(r)$ with decreasing temperature can be related to an evolution of topological short-range order [49]. To better quantify topological evolutions as a function of temperature, we then determined local ordering around each component using the common-neighbor analysis.

2. *Common-neighbor analysis*

Among the methods to get a three-dimensional picture of the local ordering surrounding each pair of atoms, common-neighbor analysis (CNA) is able to discriminate between various local topologies like fcc, hcp, bcc, and icosahedral, as well as more complex polytetrahedral environments. The classification of each pair of atoms according to the number and topology of their common neighbors is done by means of a set of four indices as described in details in our preceding papers [49,50].

To perform CNA at a given temperature, we have first selected ten configurations regularly spaced in time and

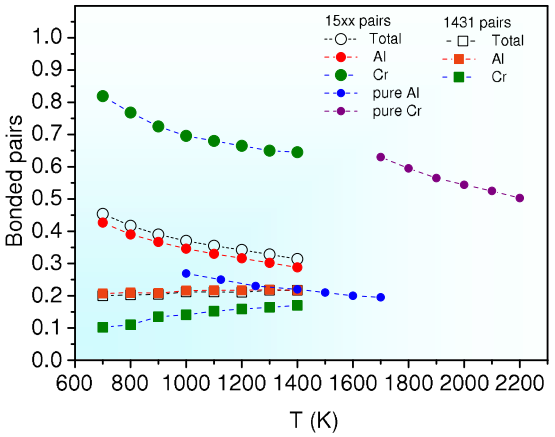

FIG. 3. Bonded pairs determined from the common-neighbor analysis as a function of temperature obtained from the common-neighbor analysis around Al and Cr atoms, as well as the total one: $15xx$ (1551+1541), and 1431. The analyses for pure Al and pure Cr are also included for comparison.

extracted their inherent structures. In this approach, the objective is to bring the configurations in local minima of the potential energy landscape (PEL) [51], so called as the inherent structure energies (ISEs). This is done numerically by carrying out a conjugate gradient energy minimization in order to suppress the kinetic energy. Therefore, the structural properties can be studied in their finer details without thermal noise.

In Fig. 3, we report the most abundant bonded pairs, the 1431 and $15xx$, representing the sum of 1551 and 1541 pairs, respectively, for the Al and Cr component in the $Al_{93}Cr_7$ alloy.

We find that the local ordering of $Al_{93}Cr_7$ is dominated by $15xx$ pairs which are representative of the icosahedral symmetry (ISRO). The comparison between two components indicates that ISRO is much more pronounced around Cr atoms and increases more rapidly upon cooling. The respective abundance of the 1431 pairs, which can be considered as either distorted icosahedra or distorted close-packed structures [52], reinforces the fact that the local environments around Al and Cr are different.

Interestingly, we also report the $15xx$ pairs for pure Cr and Al liquids in Fig. 3. We observe that the ISROs of Al and Cr in $Al_{93}Cr_7$ are quite different from those observed in pure Cr and Al liquids, which is still an indication of the strong interplay between CSRO and ISRO.

Furthermore, as the formation of medium-range order in the undercooled state refers to Cr atoms, we can conclude that such MRO displays a strong icosahedral bond-orientational order (IMRO). It is illustrated in the left panel of Fig. 2 in which two typical Cr-centered icosahedra are highlighted in yellow for visual purposes. How such IMRO can be compared to structural models proposed by Laws *et al.* [53] is beyond the scope of the present study.

B. Dynamic properties

One of the main objectives of this work concerns the investigation of single-particle dynamics and the related relaxation phenomena upon cooling in $Al_{93}Cr_7$. Self-diffusion coefficients are characterized by the individual atom displacement through the mean-square displacement for each species i (i = Al or Cr),

$$R_i^2(t) = \frac{1}{N_i}\sum_{k=1}^{N_i}\langle[\mathbf{r}_k(t+t_0)-\mathbf{r}_k(t_0)]^2\rangle_{t_0}, \quad (1)$$

where $\mathbf{r}_k(t)$ represents the position of atom k of species i at time t. The angular brackets represent the average over time origins t_0. The self-diffusion coefficient D_i can be determined from the long time slope of $R_i^2(t)$, namely,

$$D_i = \lim_{t\to\infty}\frac{R_i^2(t)}{6t}. \quad (2)$$

Relaxation phenomena can be studied through the structural relaxation time. To obtain this quantity, we start from the self-part of the van Hove (vH) function that is defined for each species i by [54]

$$G_{s,i}(r,t) = \frac{1}{N_i}\left\langle\sum_{k=1}^{N_i}\delta[r-|\mathbf{r}_k(t+t_0)-\mathbf{r}_k(t_0)|]\right\rangle_{t_0}. \quad (3)$$

The function $G_S(r,t)$ gives a measure of the probability that a given particle has undergone a displacement r after a time t from the time origin t_0 . Spatial Fourier transform of $G_S(r,t)$ yields the self-intermediate scattering function

$$F_{s,i}(q,t) = \frac{1}{N_i}\left\langle\sum_{k=1}^{N_i}\exp\{i\mathbf{q}[\mathbf{r}_k(t+t_0)-\mathbf{r}_k(t_0)]\}\right\rangle_{t_0}, \quad (4)$$

where $\mathbf{q} = (2\pi/L)(n_x,n_y,n_z)$ are wave vectors compatible with the length $L = V^{1/3}$ of the simulation cell and n_x,n_y, and n_z are integers. At long times, $F_S(q,t)$ should undergo a final decay, known as the α-relaxation process characteristic of the diffusive regime, from which the structural relaxation time τ_α can be determined [54].

1. Self-diffusion coefficients

We start our analysis of the dynamic properties with the diffusion properties through the mean-square displacements (MSDs), which are commonly drawn in the log-log scale in Figs. 4(a) and 4(b), respectively, for Al and Cr. The curves are shown for temperatures ranging from $T = 1400$ K in the stable liquid to $T = 700$ K in the deep undercooling. For both components, MSDs display common characteristic features with a ballistic regime at short times, where an atom does not encounter any other atoms in its vicinity. In this case, the distance traveled is linearly proportional to the time interval considered, and thus MDS is proportional to t^2. Beyond the ballistic motions, there is a plateau that is much more pronounced at lower temperatures and indicative of the onset of a caging effect. Finally, at longer times, atoms collide with one another and in this regime MSD enters linear behavior as a function of time corresponding to a diffusive regime. It is worth mentioning that MSD curves for Cr atoms display some small oscillations around the linear behavior at long times. This is due to the statistics which is not as good as the one for Al, the number of Cr atoms being small. The progressive shift of MSD curves to larger times upon cooling indicates a decrease of the self-diffusion coefficient.

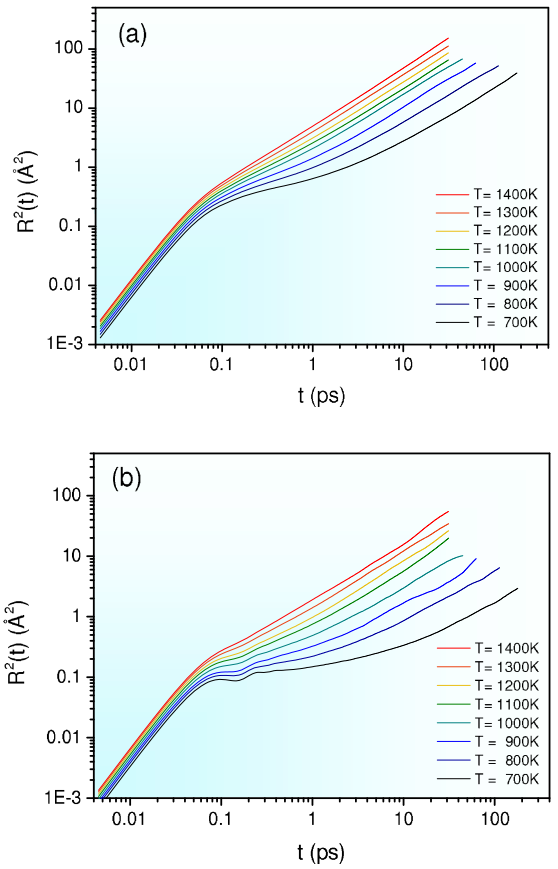

FIG. 4. Mean-square displacement for all investigated temperatures for Al atoms (a) and Cr atoms (b).

A comparison of Figs. 4(a) and 4(b) reveals that the MSD of Al is the largest and that of Cr is the smallest, whatever the temperature. In the undercooled regime, a more pronounced cage effect for Cr than for Al is observed, and therefore increases the difference between the diffusion of two components.

In Fig. 5, we show the temperature dependence of D_{Al} and D_{Cr} in $Al_{93}Cr_7$ as well as those of pure Al and Cr liquids. In the alloy, their inverse temperature dependence displays

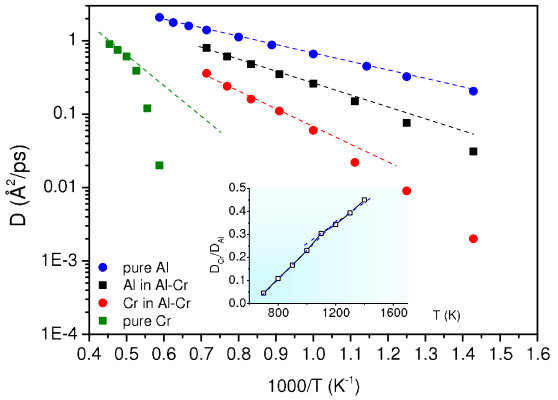

FIG. 5. Arrhenius plot of the Al and Cr self-diffusion coefficients as well as for pure liquid Al and pure Cr atoms. Dashed lines are the Arrhenius fit in the high-temperature range.

an Arrhenius-type behavior at high temperatures while we detect a sharp deviation from the Arrhenius fit below 1000 K. This is indicative of the onset of correlated dynamics of the system, where the system transitions from a state with the uncorrelated liquid dynamics at high temperatures to a state with increasing cooperativity in various regions in time and space [10].

Interestingly, the ratio between the two self-diffusion coefficients displayed in the inset of Fig. 5 reveals that Cr dynamics is clearly decoupled from Al and this decoupling is accelerated below 1000 K. This decoupling can be attributed to local orderings around Al and Cr which become more and more different upon cooling, through the interplay between CSRO and ISRO as discussed above. As a matter of fact, icosahedral motifs are known to be the most compact local structures and consequently they favor the caging effect [55]. This decoupling of dynamics can also be an important mechanism causing heterogeneous dynamics [4] as it will be seen below.

Finally, the influence of local ordering on self-diffusion coefficients is also seen in Fig. 5 through the comparison of self-diffusion of both components in the alloy with those of pure liquids. We find a strong increase of D_{Cr} upon alloying while we observe the opposite for D_{Al}, which can be still connected to the important alloying effects in $Al_{93}Cr_7$. As expected, these alloying effects impact more strongly minority atoms, Cr, than majority ones, Al.

2. *Structural relaxation*

We now examine the self-intermediate scattering function (SISF) that gives additional information on liquid $Al_{93}Cr_7$ concerning the structural relaxation. Figures 6(a) and 6(b) show the temperature dependence of SISF drawn as a function of time in the log scale, for each component. We have considered a wave number $q = 2.75\,\text{Å}^{-1}$ corresponding to the position of the first peak of the structure factor $S(q)$ (not shown) [56]. At short times, typically below 0.1 ps, SISF shows a Gaussian-like behavior indicative of the ballistic regime. In the high-temperature range, it is followed by an exponential decay which is an indication of a homogeneous diffusion regime. At lower temperatures, in the undercooled region, SISF reveals two relaxation mechanisms separated by a shoulder corresponding to the plateau in MSD. The early relaxations are usually referred to as the so-called β-relaxation regime while the final decay from this shoulder to zero corresponds to a slower relaxation process referred as the so-called α relaxation. At low temperature, we can see that the decay to zero of SISF is more rapid for Al, indicating that the structural relaxation is faster for this component. This is consistent with the faster diffusion of Al observed in MSD.

The α-relaxation time, τ_α, is obtained at the time needed for the corresponding self-intermediate scattering function $F_s(q,t)$ at the first peak of $S(q)$ to be equal to $1/e$ as was done in Ref. [57]. The deviation from a simple Arrhenius behavior is easily observed in Fig. 7 plotted in a semilogarithmic scale. It is interesting to note that the deviation of τ_α from the Arrhenius behavior is observed around $T = 1000$ K for Cr while it occurs around 800 K for Al.

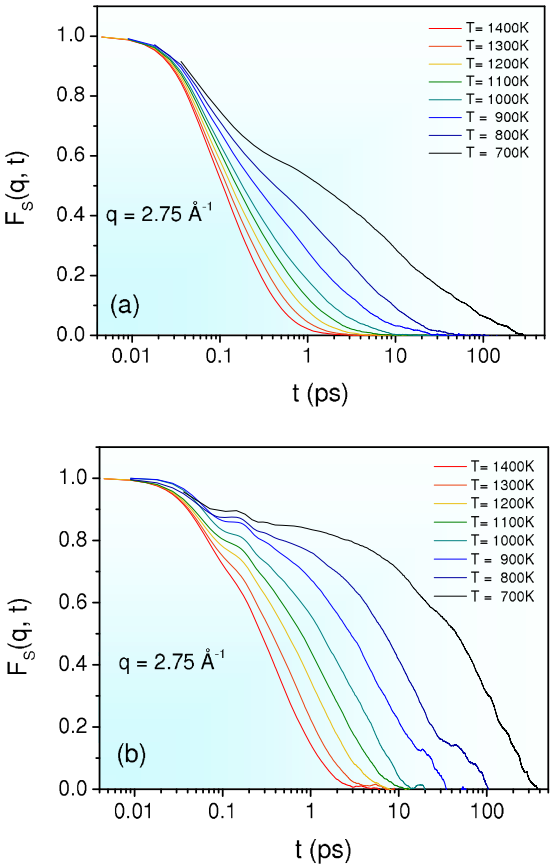

FIG. 6. Self-intermediate scattering functions for all investigated temperatures for Al atoms (a) and Cr atoms (b). The chosen q values of 2.75 Å^{-1} correspond to the position of the total structure factor maximum.

C. Dynamical decoupling and dynamic heterogeneities

1. Decoupling of elemental dynamics

Single-particle dynamics of components occurs in various time scales. This can be readily quantified by taking the ratio of self-diffusion coefficients and the relaxation times of Al and Cr as shown in Fig. 8. Al and Cr diffusion and relaxations are observed to clearly decouple even at high temperatures, in the liquid regime. For instance, the ratio of $D_{\mathrm{Al}}/D_{\mathrm{Cr}}$ is found to be roughly equal to 3 at the liquidus temperature and the decoupling is strongly accelerated below this temperature.

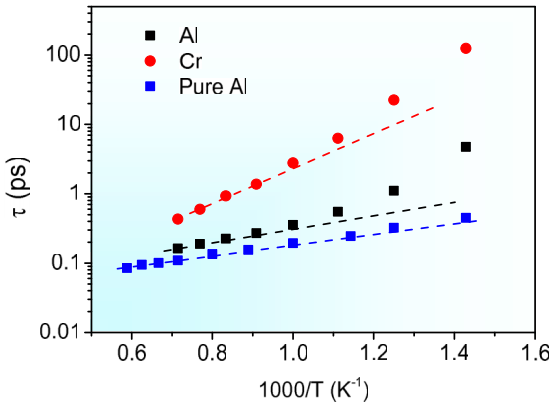

FIG. 7. Arrhenius plot of the α-structural relaxation time for Al and Cr. The values for Al are also included for comparison. The dashed line corresponds to the Arrhenius fit in the high-temperature range.

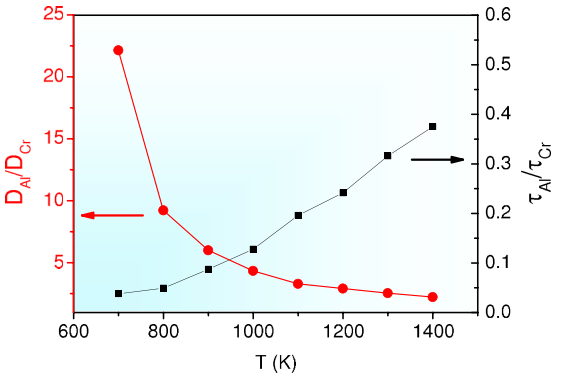

FIG. 8. Ratio of the self-diffusion coefficients as well as the α-structural relaxation times of the components for Al and Cr.

We observe the same trend for the ratio of α-relaxation times even if this ratio gives evidence of a much larger α-relaxation time for the heavy Cr atoms as expected. More interesting would be the determination of the ratio between the α-relaxation time of Al atoms located in the IMRO-based region and that of Al atoms outside this region. However, due to the ergodic character of the system at the temperatures we study, Al atoms in IMRO can move in the other region and vice versa, leading to some difficulty of determining this ratio quantitatively. Therefore, in Fig. 7, we report the α-relaxation time of Al in pure liquid Al and from comparison with the α-relaxation time of Al in $Al_{93}Cr_7$ we can determine the effect of Cr addition. In particular, we observe a strong difference at low temperatures due to the non-Arrhenius behavior of the α-relaxation time of Al in $Al_{93}Cr_7$. Therefore, we can attribute the departure from the Arrhenius law to Al atoms located in IMRO and we evidence, although indirectly, that Al atoms in the IMRO-based region have a higher α-relaxation time than that of Al atoms outside this region.

We can then suspect that the decoupling of dynamics between the two components can be an important mechanism causing heterogeneous dynamics in $Al_{93}Cr_7$ in the undercooled state.

2. Breakdown of the Stokes-Einstein relation

Having computed both self-diffusion coefficients and structural relaxation times, we can test the validity of the Stokes-Einstein (SE) relation. The latter provides a simple connection between the diffusion coefficients and the relaxation time through $D \sim (\tau_\alpha/T)^{-1}$ that works remarkably well for many liquids over a wide range of temperatures. In the undercooling regime, a decoupling leads to a violation of the SE relation [10]. Figure 9 shows the evolution of the ratio $y = D\tau_\alpha/T$ as a function of temperature for both Al and Cr. It can be seen that the SE relation is obeyed up to 1000 K for each component, as y remains essentially constant. The temperature derivative of y drawn in the inset of Fig. 9 reveals that the breakdown becomes significant below $T = 1000$ K which corresponds

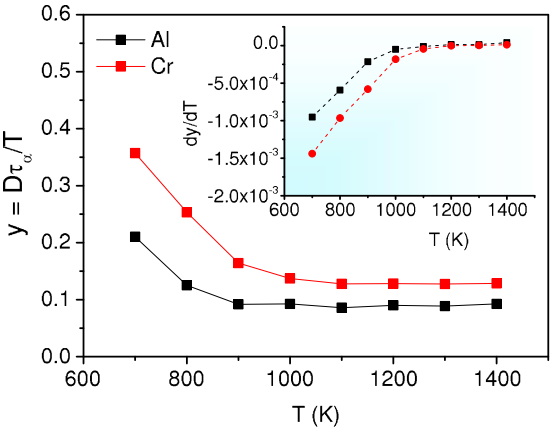

FIG. 9. Stokes-Einstein ratio $y = D\tau_\alpha/T$ as a function of temperature for Al and Cr atoms. Inset: Temperature derivative dy/dT for Al and Cr atoms as a function of temperature.

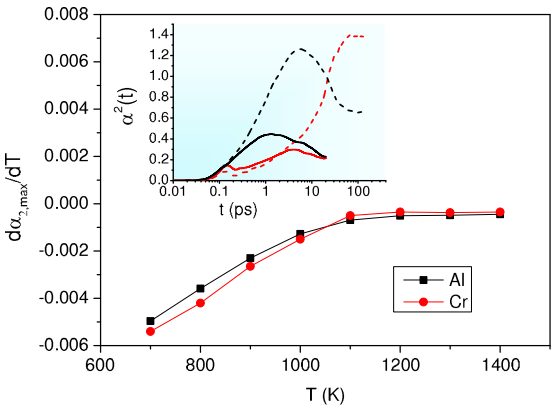

FIG. 10. Temperature derivative $d\alpha_2^{\max}/dT$ for Al and Cr atoms as a function of temperature. Inset: Non-Gaussian parameter of Al and Cr for temperatures $T = 1100$ K (solid lines) and 700 K (dashed lines).

roughly to the crossover from Arrhenius to non-Arrhenius behavior observed for both self-diffusion coefficients and structural relaxation times.

3. Non-Gaussian parameter

The decoupling between diffusion and relaxation time is often related to dynamic heterogeneities (DHs) [10], denoting higher and lower mobility of atoms with respect to the long time average in which an equal mobility of all the atoms is recovered. Therefore, the onset of the growth of DHs is considered to be at the origin of the breakdown of the SE relation [58–60]. However, some other studies found no connection between the breakdown of SE and DHs [8,12]. To address this question for the metallic $Al_{93}Cr_7$ liquid we quantify DHs by means of the non-Gaussian parameter [61] defined as

$$\alpha_2(t) = 3R^4(t)/5[R^2(t)]^2 - 1, \tag{5}$$

where $R^2(t)$ and $R^4(t)$ are, respectively, the mean-square displacement given by Eq. (1) and mean-quadruple displacement. Typically, $\alpha_2(t)$ reaches a maximum value $\alpha_2^{\max}$ around 0.2 on the subpicosecond scale due to the anisotropy of atomic motions in the ballistic regime. Then, a rapid decrease towards zero, inversely proportional to time, is observed at long times, which is an indication of a homogeneous diffusive regime. Otherwise, an increase of the amplitude of $\alpha_2^{\max}$ above 0.2 is associated to an increasing degree of DHs.

In Fig. 10, we display the evolution of the temperature derivative of $\alpha_2^{\max}$ for Al and Cr while in the inset, we plot the curves of $\alpha_2(t)$ for two temperatures, which are characteristic of the high-temperature regime and the undercooled regime, $T = 1100$ and 700 K, respectively. Below 1000 K our findings indicate a strong temperature dependence of $d\alpha_2^{\max}/dT$ for the two components, indicating that DHs grow with an increasing rate in the undercooled regime. Then we find that in $Al_{93}Cr_7$, DHs emerge almost at the same temperature as the breakdown of the SE relation.

4. Spatial distribution of dynamic heterogeneities

In a multicomponent alloy, the spatially dynamic heterogeneity is believed to be initiated by the varying mobility of each component that forms clusters and moves cooperatively. However, a physical picture in the atomic scale is yet not fully developed [4] and is unlikely to have a universal answer [59,61]. Because of the highly localized nature of cooperative dynamics, it is necessary to establish relevant quantity that distinguishes local fluctuations in atomic positions and velocities [62]. One particularly useful simulation-based tool for quantifying the influence of structure on dynamics is the isoconfigurational ensemble where many molecular dynamics simulations are performed starting from the same initial configuration but with momenta sampled randomly from a Boltzmann distribution [31–33]. Each molecular dynamics simulation is performed for an equal time interval, of the order of τ_α, to permit the observation of DHs, and the MSD is calculated for each atom. The atom's propensity for displacement is then defined from the averaging of MSD of each atom over the various simulations, where a higher value of propensity indicates greater mobility of atoms. In this manner, spatial heterogeneities are immediately evident with the reasonable assumption that particles with low propensity have a larger measure of local structural stability.

To quantify the spatial distribution of the $Al_{93}Cr_7$ dynamic heterogeneity, we performed simulations in the isonfigurational ensemble at the undercooled temperature, $T = 800$ K. Starting from the same initial configuration, isoconfiguration analysis was conducted using 50 *NVT* simulations with different initial velocities drawn randomly from a Maxwell-Boltzmann distribution. To permit the observations of DHs, the time of each simulation was equal to four times the α-structural relaxation time, τ_α, computed above. The mean-square displacements for each isoconfiguration were measured and averaged for each atom in order to correlate the atom's propensity for displacement to its local structural order. The propensity map is shown in Fig. 11(a). From inspection, we note that the heterogeneous structure of $Al_{93}Cr_7$ at $T = 800$ K is well pronounced in both the localized sites of high propensity and the extended domains of low propensity. In

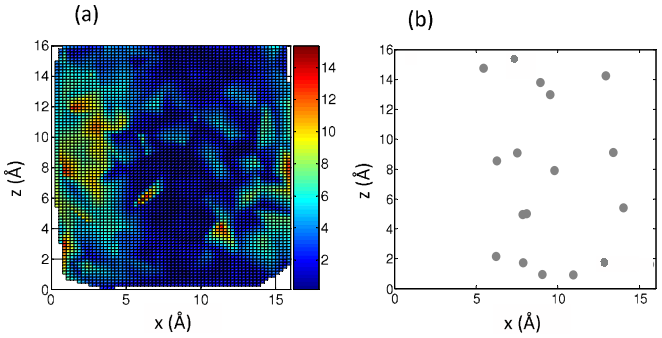

FIG. 11. (a) Propensity map of all atoms in the simulation box at $T = 800\,\mathrm{K}$. The color scale corresponds to the propensity in angstroms squared. (b) Positions of the Cr atoms in the initial configuration of the isoconfiguration ensemble simulations (see text). In both panels the positions of Cr atoms are projected onto the x-z plane.

Fig. 11(b), we report the spatial distribution of Cr atoms in the alloy. Interestingly, from comparison with Fig. 11(a), we observe that Cr atoms are present only in the domains of low propensity. Then we can conclude that IMRO induced by the correlated Cr atoms via the strong Al-Cr affinity is responsible for slow dynamics while localized fast-dynamic regions are formed by Al atoms only, those which are not involved in the IMRO-based region.

Finally, we note that that IMRO may play a key role in the quasicrystal-enhanced nucleation mechanism observed recently in Al-Zn alloys with Cr additions [38,39]. Indeed, Kurtuldu *et al.* have examined in detail how nucleation of Al grains might occur when Cr is added to liquid Al-Zn alloys [38]. The authors assume a process that may resemble spinodal decomposition, where added Cr develops local concentration at which there is icosahedral ordering of atoms in the liquid. Such a cluster grows into an icosahedral phase or a fragment of the approximant Al_7Cr phase [63] which acts then as a template for the formation of many Al grains having twin or near-twin relationships between them. Within this approach, preexisting icosahedral solid clusters promote the formation of the crystalline Al phase even though no icosahedral or the approximant stable Al_7Cr phase was detected in the experimental study. To explain this absence, Kurtuldu *et al.* assume that the preexisting or primary phase undergoes a peritectic reaction with the liquid to give the final Al phase.

From our study, we can imagine a slightly different scenario: IMRO-based regions enriched in Cr may lead to the formation of transient structures which could act as a nucleation center for the rest of the Al atoms since their dynamics is much slower than that of Al atoms upon cooling. However, we cannot exclude the formation of Al_7Cr as a primary phase since the chemical composition as well as the fivefold symmetry of the IMRO-based regions are in close correspondence with this phase. In both cases, our findings would support that icosahedra in a metallic liquid could be regarded also as a structural motif linked to the formation of a crystalline ground state as already proposed by Tanaka [23] and not only at the origin of frustration leading to the glass formation [22].

IV. CONCLUSION

In summary, we have performed a series of *ab initio* molecular dynamics simulations in order to evidence the striking effects of Cr alloying on structural and dynamic properties of liquid and undercooled $Al_{93}Cr_7$ alloy.

The local ordering evolutions are examined through the partial pair-correlation functions and abundance of bonded pairs by means of the common-neighbor analysis. Our results indicate that the local structure is characterized by a strong Al-Cr affinity which favors the occurrence of the ISRO around Cr atoms, leading to different local ordering around Al and Cr. In the undercooled regime, below 1000 K, we observe the formation of an icosahedral-based medium-range order (IMRO) referring to Cr atoms. This formation with the strong intermixing between Cr and Al atoms increases the atomic-scale heterogeneity because Al atoms as the first-nearest neighbors of Cr atoms are less than Al atoms expected from the alloy composition.

Then, we evidence the evolution of this chemically induced structural heterogeneity on dynamic properties like the self-diffusion coefficients and relaxation times.

We obtain that Al and Cr diffusion and relaxations strongly decouple even at high temperatures, in the liquid regime. For instance the ratio of $D_{\mathrm{Al}}/D_{\mathrm{Cr}}$ is found to be roughly equal to 3 at the liquidus temperature, 1000 K, and the decoupling is strongly accelerated below this temperature. Such a decoupling is also observed for the α-relaxation time with, however, a less dramatic evolution at low temperature.

We find that $T = 1000\,\mathrm{K}$ corresponds roughly to a crossover behavior from an Arrhenius to a non-Arrhenius-temperature evolution of diffusivity and relaxation time. Moreover we show that this temperature is also the onset of DHs via the breakdown of the SE relation and the increase of the non-Gaussian parameter.

To quantify the spatial distribution of the $Al_{93}Cr_7$ dynamic heterogeneity, we performed simulations in the isonfigurational ensemble at the undercooled temperature, $T = 800\,\mathrm{K}$. From the propensity map, we observe that the heterogeneous structure of $Al_{93}Cr_7$ at $T = 800\,\mathrm{K}$ is well pronounced in both the localized sites of high propensity and the extended domains of low propensity. Moreover, we find that IMRO induced by the correlated Cr atoms via the strong Al-Cr affinity is responsible for slow dynamics while localized fast-dynamic regions are formed by Al atoms only.

Finally, the present *ab initio* simulations suggest that chemically induced structural heterogeneities that promote dynamic heterogeneities may also have an important implication in a quasicrystal-based nucleation mechanism of multiply twinned Al grains. What the relationship is between these two phenomena needs, however, a more detailed study.

ACKNOWLEDGMENTS

We acknowledge the CINES and IDRIS under Project No. INP2227/72914 as well as PHYNUM CIMENT for computational resources. This work was performed within the framework of the Centre of Excellence of Multifunctional Architectured Materials "CEMAM" No. ANR-10-LABX-44-01 funded by the "Investments for the Future" Program.

[1] C. A. Angell, Science **267**, 1924 (1995).
[2] T. Hecksher, A. I. Nielsen, N. B. Olsen, and J. Dyre, Nat. Phys. **4**, 737 (2008).
[3] H. Silescu, J. Non-Cryst. Solids **243**, 81 (1999).
[4] M. D. Ediger, Annu. Rev. Phys. Chem. **51**, 99 (2000).
[5] C. A. Angell, K. Ngai, G. B. McKenna, P. F. McMillan, and S. W. Martin, J. Appl. Phys. **88**, 3113 (2000).
[6] R. Richert, J. Phys.: Condens. Matter **14**, R703 (2002).
[7] P. G. Debenedetti and F. H. Stillinger, Nature **410**, 259 (2001).
[8] H. C. Andersen, Proc. Natl. Acad. Sci. USA **102**, 6686 (2005).
[9] M. D. Ediger and P. Harrowell, J. Chem. Phys. **137**, 080901 (2012).
[10] L. Berthier and G. Biroli, Rev. Mod. Phys. **83**, 587 (2011).
[11] S. K. Kumar, G. Smazel, and J. F. Douglas, J. Chem. Phys. **124**, 214501 (2006).
[12] S. R. Becker, P. H. Poole, and F. W. Starr, Phys. Rev. Lett. **97**, 055901 (2006).
[13] K. L. Ngai, J. Phys. Chem. B **103**, 10684 (1999).
[14] N. Jakse and A. Pasturel, Phys. Rev. B **94**, 224201 (2016).
[15] M. G. Mazza, N. Giovambattista, F. W. Starr, and H. E. Stanley, Phys. Rev. Lett. **96**, 057803 (2006).
[16] H. Jonsson and H. C. Andersen, Phys. Rev. Lett. **60**, 2295 (1988).
[17] T. Tomida and T. Egami, Phys. Rev. B **52**, 3290 (1995).
[18] A. Malins, J. Eggers, C. P. Royall, S. R. Williams, and T. Tanaka, J. Chem. Phys. **138**, 12A535 (2013).
[19] C. P. Royall, S. R. Williams, T. Ohtsuka, and H. Tanaka, Nat. Mater. **7**, 556 (2008).
[20] R. G. Della Valle, D. Gazzillo, R. Frattini, and G. Pastore, Phys. Rev. B **49**, 12625 (1994).
[21] F. C. Frank, Proc. R. Soc. London, Ser. A **215**, 43 (1952).
[22] G. Tarjus, S. A. Kivelson, Z. Nussinov, and P. Viot, J. Phys.: Condens. Matter **17**, R1143 (2005).
[23] H. Tanaka, Eur. Phys. J. E: Soft Matter Biol. Phys. **35**, 113 (2012).
[24] D. Coslovich and G. Pastore, J. Chem. Phys. **127**, 124504 (2007).
[25] U. R. Pedersen, T. B. Schrøder, J. C. Dyre, and P. Harrowell, Phys. Rev. Lett. **104**, 105701 (2010).
[26] H. Shintani and H. Tanaka, Nat. Phys. **2**, 200 (2006).
[27] M. Leocmach and H. Tanaka, Nat. Commun. **3**, 974 (2012).
[28] X. J. Han, J. G. Li, and H. R. Schober, J. Chem. Phys. **144**, 124505 (2016).
[29] H. Teichler, Phys. Rev. Lett. **107**, 067801 (2011).
[30] S. D. Feng, L. Qi, L. M. Wang, P. F. Yu, S. L. Zhang, M. Z. Ma, X. Y. Zhang, Q. Jing, K. L. Ngai, A. L. Greer, G. Li, and R. P. Liu, Scr. Mater. **115**, 57 (2016).
[31] A. Widmer-Cooper, P. Harrowell, and H. Fynewever, Phys. Rev. Lett. **93**, 135701 (2004).
[32] A. Widmer-Cooper and P. Harrowell, Phys. Rev. Lett. **96**, 185701 (2006).
[33] A. Widmer-Cooper, H. Perry, P. Harrowell, and D. R. Reichman, Nat. Phys. **4**, 711 (2008).
[34] M. S. Razul, G. S. Matharoo, and P. H. Poole, J. Phys.: Condens. Matter **23**, 235103 (2011).
[35] K. D. Vargheese, A. Tandia, and J. C. Mauro, J. Chem. Phys. **132**, 194501 (2010).
[36] P. A. Bancel and P. A. Heiney, Phys. Rev. B **33**, 7917 (1986).
[37] L. C. Chen and F. Spaepen, Nature **336**, 366 (1988).
[38] G. Kurtuldu, P. Jarry, and M. Rappaz, Acta Mater. **61**, 7098 (2013).
[39] G. Kurtuldu, P. Jarry, and M. Rappaz, Acta Mater. **115**, 423 (2016).
[40] G. Kresse and J. Furthmüller, Comput. Mater. Sci. **6**, 15 (1996).
[41] D. M. Ceperley and B. J. Alder, Phys. Rev. Lett. **45**, 566 (1980); J. P. Perdew and A. Zunger, Phys. Rev. B **23**, 5048 (1981).
[42] N. Jakse and A. Pasturel, Sci. Rep. **3**, 3135 (2013).
[43] M. Trybula, N. Jakse, W. Gasior, and A. Pasturel, J. Chem. Phys. **141**, 224504 (2014).
[44] N. Jakse and A. Pasturel, J. Chem. Phys. **144**, 244502 (2016).
[45] J. D. Honeycutt and H. C. Andersen, J. Phys. Chem. **91**, 4950 (1987).
[46] J.-P. Hansen and I. R. McDonald, *Theory of Simple Liquids*, 2nd ed. (Academic Press, London, 1986).
[47] M. P. Allen and D. J. Tildesley, *Computer Simulation of Liquids* (Oxford University Press, Oxford, 1989).
[48] M. Maret, T. Pomme, A. Pasturel, and P. Chieux, Phys. Rev. B **42**, 1598 (1990).
[49] N. Jakse and A. Pasturel, Mod. Phys. Lett. B **20**, 655 (2006).
[50] N. Jakse and A. Pasturel, Phys. Rev. Lett. **91**, 195501 (2003).
[51] F. H. Stillinger and T. A. Weber, Phys. Rev. A **25**, 978 (1982).
[52] L. van Hove, Phys. Rev. **95**, 249 (1954).
[53] K. J. Laws, D. B. Miracle, and M. Ferry, Nat. Commun. **6**, 8123 (2015).
[54] K. Binder and W. Kob, *Glassy Materials and Disordered Solids* (World Scientific Publishing, Singapore, 2005).
[55] A. Pasturel, E. S. Tasci, M. H. F. Sluiter, and N. Jakse, Phys. Rev. B **81**, 140202(R) (2010).
[56] N. Jakse and A. Pasturel, J. Chem. Phys. **143**, 084508 (2015).
[57] S. K. Das, J. Horbach, and T. Voigtmann, Phys. Rev. B **78**, 064208 (2008).
[58] J. F. Douglas and D. Leporini, J. Non-Cryst. Solids **235–237**, 137 (1998).
[59] A. Jaiswal, T. Egami, and Y. Zhang, Phys. Rev. B **91**, 134204 (2015).
[60] K. N. Lad, N. Jakse, and A. Pasturel, J. Chem. Phys. **136**, 104509 (2012).
[61] T. Fujita, P. F. Guan, H. W. Sheng, A. Inoue, T. Sakurai, and M. W. Chen, Phys. Rev. B **81**, 140204(R) (2010).
[62] F. Faupel, M. P. Macht, H. Mehrer, V. Naundorf, K. Rätzke, H. R. Schober, S. K. Sharma, and H. Teichler, Rev. Mod. Phys. **75**, 237 (2003).
[63] M. J. Cooper, Acta Crystallogr. **13**, 257 (1960).